Acta. Chim. Asiana., 2023, 6(1), 269 –278
e-ISSN/p-ISSN 2550-0503/2550-049x
Available online at: www.aca.unram.ac.id

RESEARCH PAPER

Free solvent isolation of Fe_3O_4 from magnetic material iron sand utilizing high-energy ball milling as adsorben remazol turquoise blue G-133 and remazol red RB-133

Muhammad Ramadhan*[a], Fahmiati Fahmiati[a b], Armid Alrum[a,b], La Ode Muhammad Zuhdi Mulkiyan[b]

[a] Postgraduate of Chemistry
Postgraduate, Halu Oleo University, Indonesia, 93121.
E-mail: muhammadramadhangolongan@gmail.com
[b] Chemistry Department
Math and Natural Science Faculty, Halu Oleo University, Indonesia, 93232.

DOI: 10.29303/aca.v6i1.143

Article info:

Received 01/01/2023

Revised 02/02/2023

Accepted 16/02/2023

Available online 18/02/2023

Abstract: The extraction of Fe3O4 from iron sand frequently utilizes a highly concentrated HCl solution, which is hazardous to the environment. The high-energy ball milling method of separating Fe3O4 from iron sand might produce Fe3O4 without acids and maintains its magnetic characteristics with a yield of 81.87%. The FTIR results suggest that the Fe3O4 separation procedure with high-energy ball milling effectively eliminated the silica pick after activation with 2 M NaOH, which was confirmed by SEM-EDS data indicating there was no silica on the material's surface. Fe3O4 was separated, allowing use as an adsorbent to treat textile industry waste, such as Remazol Turquoise Blue G-133 and Remazol Red RB-133. The adsorption of Fe3O4 on these two dyes occurred at pH 5, and as adsorbate concentration, contact time, and adsorption temperature of Fe3O4 were raised, the adsorption capacity increased. Remazol Turquoise Blue G-133 and Remazol Red RB-133 have qmax values of 16.75 and 1.43 mg/g, respectively. The isothermal adsorption of Fe3O4 for the two dyes follows the Freundlich isothermal with KF values of 1.87 and 0.42 L/g and n values of 2.17 and 1.22; respectively, results suggest that the adsorption process occurs physically and forms a multilayer adsorption surface. These results are supported by data obtained from the adsorption kinetics, which shows that it follows the first-order adsorption kinetics. The dyes thermodynamics also showed positive results for ΔHo and ΔGo, indicating that the adsorption process was endothermic and not spontaneous, but to the degree of disorder (ΔSo), Remazol Turquoise Blue G-133 outperformed Remazol Red RB-133.

Keywords: Adsorption, Remazol, Ball-milling, Fe_3O_4, Equilibrium

Citation: Ramadhan, M., Fahmiati, F., Alrum, A., & La Ode Muhammad Zuhdi, M. (2023). Free solvent isolation of Fe3O4 from magnetic material iron sand utilizing high-energy ball milling as adsorben remazol turquoise blue G-133 and remazol red RB-133. Acta Chimica Asiana, 6(1), 269–278.

INTRODUCTION

The extraction of Fe3O4 with HCl is still a common way to isolate Fe3O4 [1, 2, 3]. Although this extraction technique is affordable and extremely effective, it also has the drawback of not being environmentally friendly. Another possibility is to use high-energy ball milling. This method was used to create nanomaterials without chemical solutions, developing suitable material structures for application [4, 5].

Free solvent Isolation Fe3O4 using high-energy ball milling has the advantage of maintaining the material's magnetic characteristics and might be utilized as a magnetic adsorbent to handle industrial wastewater from the mining and textile sectors. The -OH group on the Fe-OH surface of Fe3O4 will act as a binding agent to adsorb the adsorbate molecules.

Wastewater from the textile industry can be handled more effectively and economically by using adsorbents. Synthetic dyes are used in the development of the textile industry, which frequently results in major environmental issues if they are not managed adequately before being released into the aquatic environment.

The textile industry uses chemical dyes in all production processes. It produces liquid waste residue from these chemical dyes, which must be treated before entering the aquatic environment. Today, azo dyes like Remazol Turquoise Blue G-133 and Remazol Red RB-133 are frequently used in the textile sector [6, 7]. These two dyes are commonly used because the colors created are more eye-catching and remain longer even after several washes. Due to the fact, these colors are non-biodegradable in the environment, their use is extremely hazardous if waste is not controlled [7]. This research aimed to compare the adsorption properties of Remazol Turquoise Blue G-133 with Remazol Red RB-133 on Fe3O4 separated via high-energy ball milling.

RESEARCH METHODOLOGY

Materials

Iron sand from Bugel Beach, Kulonprogo, Yogyakarta, Indonesia NaOH (R&M Chemicals), dyes Remazol Red RB-133 (Merck) and Remazol Turquoise Blue G-133 (Merck), Ethanol (Merck) and distilled water.

Tools for Analysis

Fourier Transform Infrared Spectrophotometer (IRPrestige-21, SHIMADZU Tokyo, Japan), UV–vis spectroscopy (Shimadzu 2450, Japan), and A Zeiss-EVO emission scanning electron microscope SEM-EDS (model Carl Zeiss, USA).

Methods

Fe_3O_4 Isolated from Iron Sand using High-energy Ball Milling

100 grams of iron sand were dried for 8 hours at 105^{o}C before being separated with an external Neodymium N50 magnet to get magnetic material (MM). 30 grams MM was break and shatter utilizing high-energy ball milling at 3500 revolutions per minute for 72 hours, and washed with 2 M NaOH and distilled water, respectively. Fe_3O_4 was dried with oven for 8 hours at 105^{o}C before being impregnated with 70% ethanol and dried in an oven for 5 hours at 105^{o}C.

Adsorption Study

The study of adsorption Fe_3O_4 against Remazol Turquoise Blue G-133 and Remazol Red RB-133 with variations of pH solution, concentration, contact duration, and temperature of adsorption. The batch approach was used for the adsorption procedure, decanted with an external magnetic field (Neodymium N50 magnet). The adsorption test solution was examined using a UV-Vis Spectrophotometer to determine adsorption capacity (q_e), adsorption efficiency (EA), isothermal, Kinetics and thermodynamics adsorption.

$$q_e = \frac{(C_0 - C_e)}{m} V \quad (1)$$

$$EA = \frac{(C_0 - C_e)}{C_0} 100\% \quad (2)$$

where C_0 and C_e initial and equilibrium adsorbate concentration (mg/L), V volume of the solution (L), and m adsorbent mass (mg), q_e (mg/g), EA (%),

RESULTS AND DISCUSSION

Adsorbent Fe_3O_4 Isolation

The high-energy ball milling utilized to isolate Fe_3O_4 from MM iron sand has the advantage to create nano-sized materials without using many chemicals and acid solutions. Impurities of SiO on the surface of iron sand are the second-most abundant ingredient in iron sand than FeO might be removed using NaOH [8]. The average yield obtained when Fe_3O_4 was extracted from iron sand by high-energy ball milling was 81.87%, as shown in Table 1.

Table 1. The yield of Fe_3O_4 from MM iron sand.

No.	MM (g)	Fe_3O_4 (g)	Yield (%)
sample 1	30	25.28	84.27
sample 2	30	24.42	81.40
sample 3	30	23.98	79.93
average		**24.56**	**81.87**

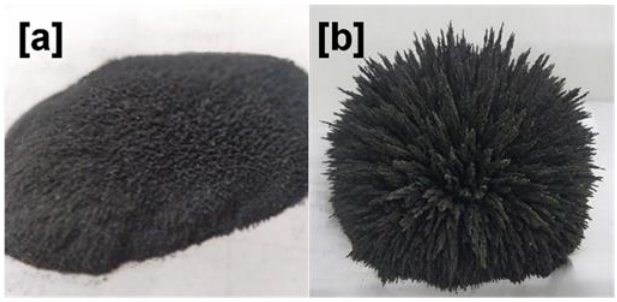

Figure 1. Physical form of (a) Iron sand and (b) Fe_3O_4.

Characterization of adsorbent

Infrared spectra (IR) analysis

FTIR spectra of Iron sands (Fig. 2.) the bending and stretching vibrations of Fe-O at wave numbers 352 and 492 cm^{-1}, respectively, and have a vibration of SiOSi and -OH at 1052 and 3454 cm^{-1}, respectively. After isolation using the method of high-energy ball milling the vibration of the silica oxide has disappeared and there has been a shift in the bending and stretching vibrations of Fe-O at wave numbers 382 and 572 cm^{-1}, in the spectra of Fe_3O_4, respectively, which was confirmed by the presence of Fe-O-Fe vibrations at wave number 892 cm^{-1} and Fe-OH at wave number 1071 cm^{-1}, which is consistent with the findings of study Elmobarak and Almomani [9].

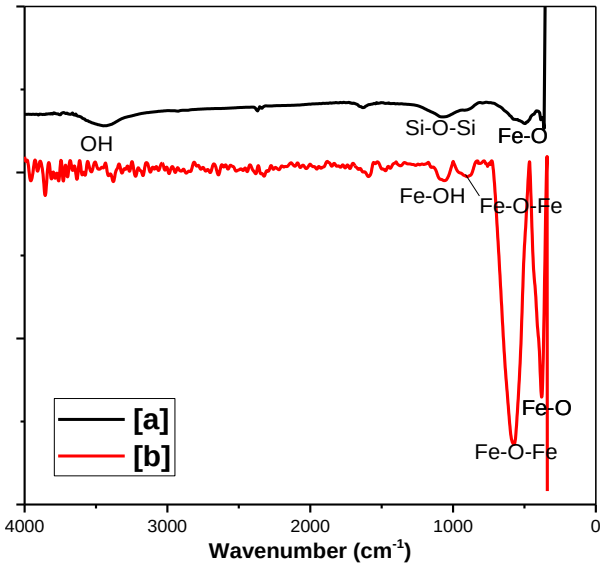

Figure 2. Functional groups characterization utilizing FTIR of (a) Iron sand and (b) Fe_3O_4

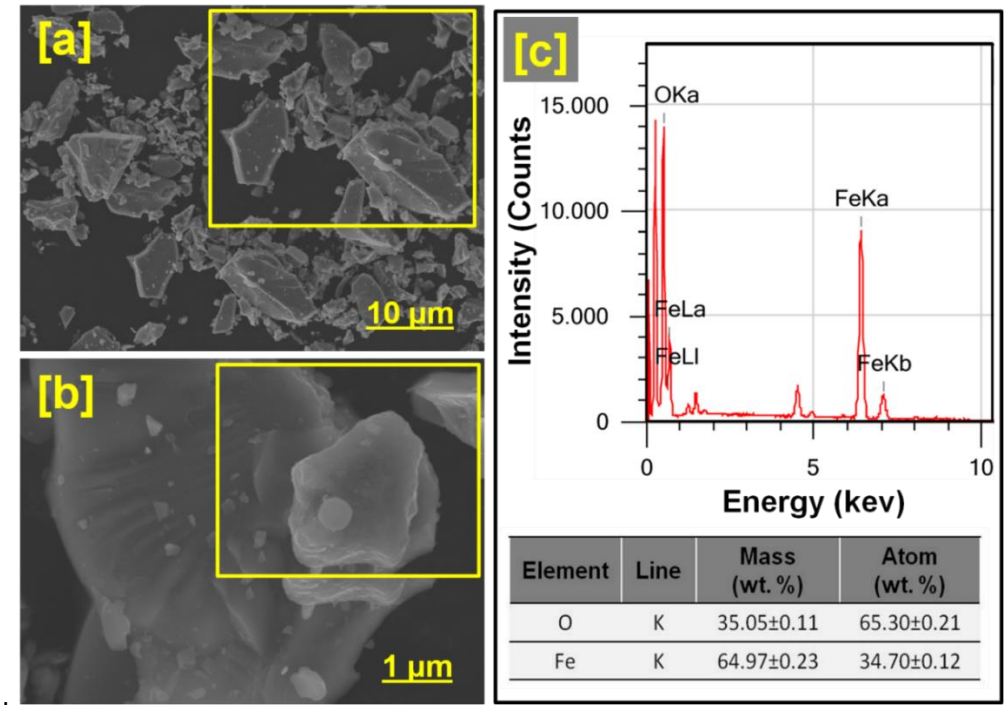

Figure 3. SEM Surface Morphology of Fe_3O_4 adsorbent (a) Lens shift of 1.000 times, (b) Lens shift of 10,000 times, and (c) EDS spectrum.

SEM-EDS analysis

To explore the surface morphology of Fe_3O_4, this research uses SEM characterization. Figure 3. shows that at a reduced magnification, a structure with lots of large grains can be seen (Figure 3.a). The precise structure of Fe_3O_4 might be observed clearly at higher magnification (see Fig. 3.b), where Fe_3O_4 is made of a spherical structure.

The elemental composition of Fe_3O_4 was investigated using EDS, with peaks corresponding to Fe and O found in the EDS spectrum. Figure 3.c depicts the EDS spectrum for the Fe_3O_4 structure, exhibiting typical elements such as Fe and O, with compositions as high as 65.30±0.21 and 34.70±0.12%, respectively. This appearance of SEM was similar to the result reported by Gunanto, et al [1], recovered Fe_3O_4 using HCl.

Figure 4.a. exhibits the SEM-EDS scan mapping of the Fe_3O_4 adsorbent material. The surface resembled a massive bulk made up of several microscopic particles. Figure 4.b-c shows the plane scan findings for the elements O and Fe; all elements are appropriately distributed on the surface.

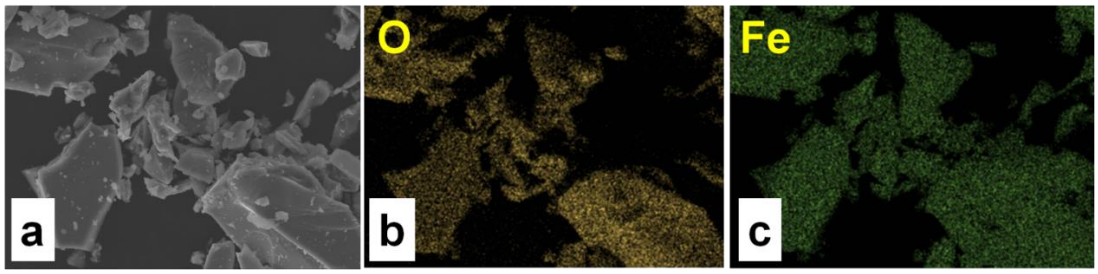

Figure 4. Plane scan analysis with SEM-EDS of Fe_3O_4 (a) SEM images (region of plane scan), (b) O content and (c) Fe content.

Adsorption study

The pH Effect

The illustrated in Fig. 5.a the quantity of solute adsorption from pH 2 to 5 has increases with rising rapidly pH and decreases when reaching a neutral to alkaline pH range (pH 6 to pH 9). The optimum pH for adsorption of Remazol Turquoise Blue G-133 and also Remazol Red RB-133 was pH 5, with q_e values of 6.96 and 6.14 mg/g and EA values of 27.87 and 25.65%, respectively. Higher adsorption at lower levels of pH might be explained by the protonation characteristics of the adsorbent increased quantity of hydrogen ions, neutralization of negative charges on the surface of interior spots, and the development of the surface produced a positive charge for anionic adsorption Remazol Turquoise Blue G-133 and Remazol Red RB-133 dye adsorption. A similar pattern of behavior has been seen for dye adsorption at several adsorbents [10, 11, 12].

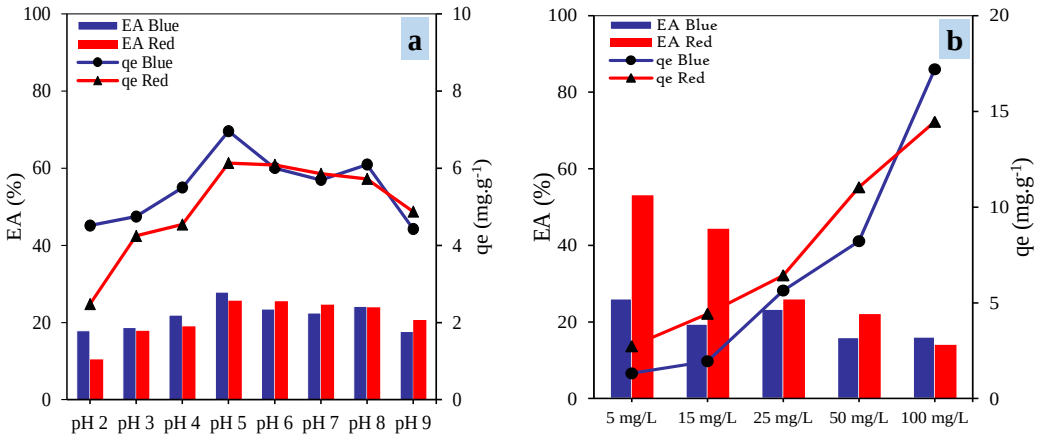

Figure 5. Capacity adsorption (q_e) and efficiency adsorption (EA) of Remazol Turquoise Blue G-133 and Remazol Red RB-133 utilizing Fe_3O_4 with variation of (a) pH and (b) concentration

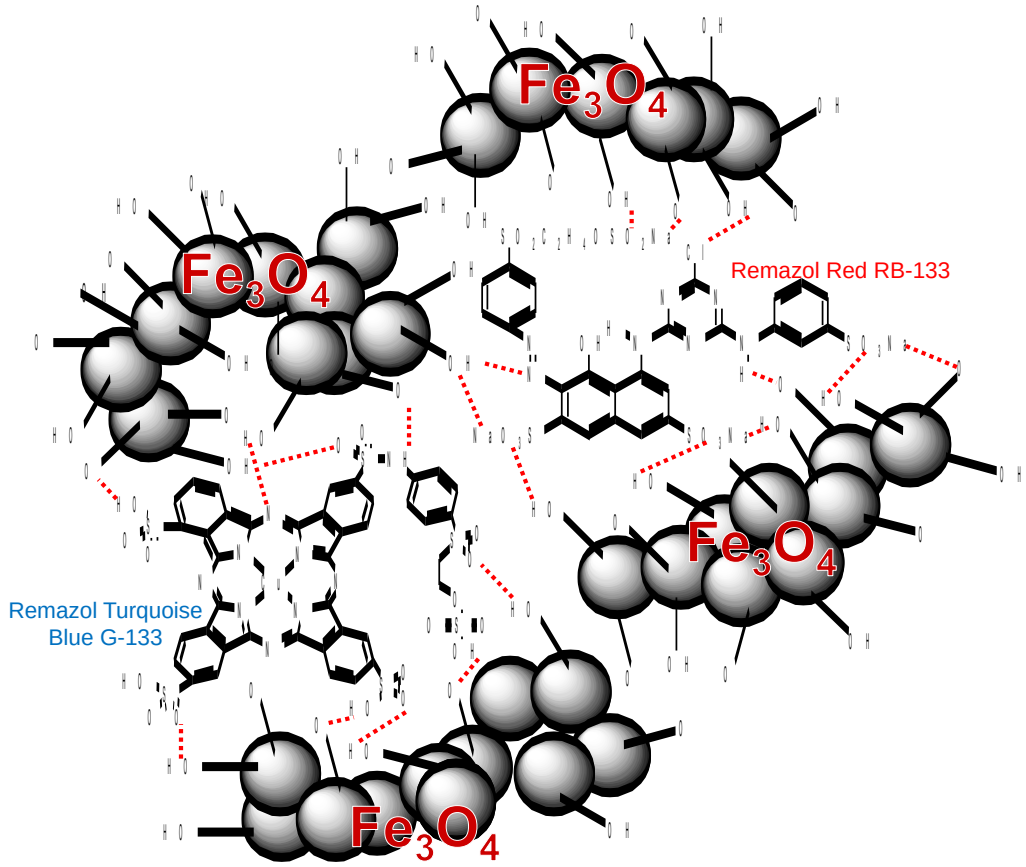

Scheme 1. Adsorption process of Remazol Turquoise Blue G-133 and Remazol Red RB-133 utilizing Fe_3O_4.

The effect of dye concentration

The impact of initial concentration on the quantity of adsorption and dye removal efficiency is shown in Fig. 5.b. Remazol Turquoise Blue G-133 and Remazol Red RB-133 absorption efficiency reached up to 26.05% and 53.06% at lower concentrations (5 mg/L), respectively, before decreasing to 16.09% and 14.0% at higher concentrations (100 mg/L). As a result of the adsorbent's availability of binding sites, the removal effectiveness of Remazol Turquoise Blue G-133 and Remazol Red RB-133 was higher at low initial concentrations. Due to various practically complete absorption of the binding sites at high dye concentrations, the EA color removal decreases with increasing dye concentrations of Remazol Turquoise Blue G-133 and Remazol Red RB-133.

The amount of dye Remazol Turquoise Blue G-133 and Remazol Red RB-133 adsorbed at equilibrium increased from 1.32 to 17.19 mg/L and 2.73 to 14.45 mg/g with initial dye concentrations increasing from 5 to 100 mg/L, respectively. The dye concentration provides the necessary driving capacity to overcome dye molecule mass transfer resistance between the aqueous and solid phases. The interaction between Remazol Turquoise Blue G-133 and Remazol Red RB-133 and materials is also enhanced by increasing the initial dye concentration. As the driving power of the concentration gradient increases, so does the dye concentration. A similar pattern was seen in the methyl orange adsorption process dye onto mesoporous carbon [13, 14].

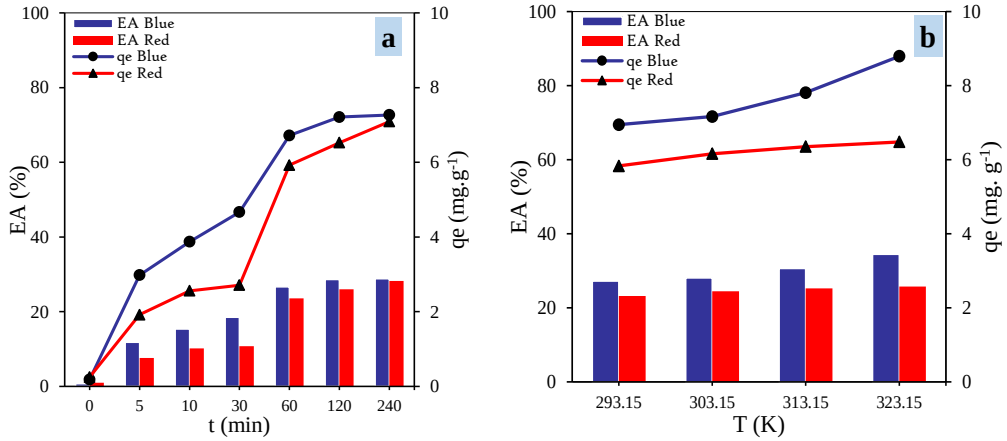

Figure 6. Capacity adsorption (q_e) and efficiency adsorption (EA) of Remazol Turquoise Blue G-133 and Remazol Red RB-133 utilizing Fe_3O_4 with variation of (a) Contact time and (b) Temperature

The Influence of Contact Time

As seen in Fig. 6.a, the time has a significant influence on dye adsorption. In the first 60 minutes, dye adsorption was relatively quick, then increased gradually with a contact time extension. There was no significant difference in adsorbed dye after 120 minutes of contact time. Based on these results, In batch adsorption studies, the equilibrium process was determined to be 120 minutes.

Effect of Temperature adsorption

The temperature has a substantial effect on dye adsorption, as seen in Fig. 6.b. The q_e and EA adsorption of Remazol Turquoise Blue G-133 and Remazol Red RB-133 increased when the temperature rises from 293.15 to 323.15 K. The q_e of Remazol Turquoise Blue G-133 increased from 69.95 mg/g at 293.15 K to 8.79 mg/g at 323.15 K, whereas the EA increased from 27.23 to 34.46 mg/g. Whereas q_e and Fe_3O_4 in Remazol Red RB-133 are lower than in Remazol Turquoise Blue G-133, optimal q_e and EA occur at 323.15 K with values of 6.48 mg/g and 25.76%, respectively.

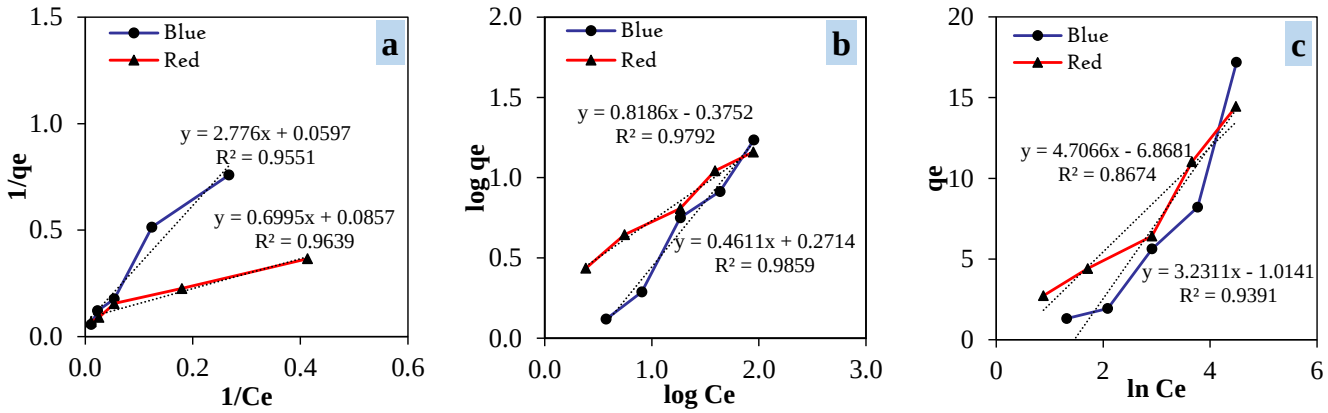

Figure 7. Isothermal adsorption of Remazol Turquoise Blue G-133 and Remazol Red RB-133 utilizing Fe_3O_4 of (a) Isothermal Langmuir, (b) Isothermal Freundlich and (c) Isothermal Temkin

Isotherm of Adsorption

Adsorption isotherms are useful for examining such interactions and predicting the retention mechanism [15]. The adsorption isotherms of Remazol Turquoise Blue G-133 and Remazol Red RB-133 using Fe_3O_4 more strongly resemble the Freundlich Isotherm for both dyes with values R^2 0.9859 dan 0.9792, respectively, with K_F values of 1.87 and 0.42 L/g and n values of 2.17 and 1.22, respectively. The q_{max} values of Remazol Turquoise Blue G-133 and Remazol Red RB-133 were 16.75 and 1.43 mg/g, respectively, based on Langmuir isothermal data. According to the acquired data, adsorption is closely follows the Freundlich isotherm, which might imply the creation of multilayer, and the adsorption process occurs physically [16].

Table 2. Isothermal coefficients of adsorption Fe_3O_4 against Remazol Turquoise Blue G-133 and Remazol Red RB-133

Isotermal models	Isothermal coefficient	Fe_3O_4
Langmuir model: $\frac{1}{q_e} = \frac{1}{K_L q_{max}} \frac{1}{C_e} + \frac{1}{q_{max}}$ linear plot: $1/q_e$ vs $1/C_e$ [17].	Remazol Turquoise Blue G-133	
	K_L ($L.mg^{-1}$)	$2.15x10^{-2}$
	q_{max} ($mg.g^{-1}$)	16.75
	Remazol Red RB-133	
	K_L ($L.mg^{-1}$)	8.16
	q_{max} ($mg.g^{-1}$)	1.43
Freundlich model: $\log q_e = \log K_F + \frac{1}{n} \log C_e$ linear plot: $\log q_e$ vs $\log C_e$ [17].	Remazol Turquoise Blue G-133	
	K_F ($L.g^{-1}$)	1.87
	N	2.17
	Remazol Red RB-133	
	K_F ($L.g^{-1}$)	0.42
	N	1.22
Temkin model: $q_e = \frac{R\,T}{b_T} \ln C_e + \frac{R\,T}{b_T} \ln K_T$ linear plot: q_e vs $\ln C_e$ [17].	Remazol Turquoise Blue G-133	
	K_T ($L.g^{-1}$)	$7.31x10^{-1}$
	b_T ($kJ.mol^{-1}$) where T (300 K)	$7.72x10^{-1}$
	Remazol Red RB-133	
	K_T ($L.g^{-1}$)	$2.32x10^{-1}$
	b_T ($kJ.mol^{-1}$) where T (300 K)	5.30x10-1

Kinetics Adsorption

Adsorption kinetics also influences adsorption rate, which determines the time required for the adsorption mechanism to reach equilibrium. Kinetic studies might provide insight on adsorption transfers and the processes that might be work. This study could be useful to process development and adsorption design process. [18].

According to Figure 8, the adsorption kinetics of Fe_3O_4 on Remazol Turquoise Blue G-133 and Remazol Red RB-133 match the first-order reaction kinetics with R^2 values of 0.9883 and 0.9415, respectively. Remazol Turquoise Blue G-133 has q_1 and K_1 values of 6.15 mg/g and $-3.92x10^{-2}$ min^{-1}, respectively. On the other hand, Remazol Red RB-133 has q_1 and K_1 values of 6.10 mg/g and $-2.10x10^{-2}$, respectively. For the two dyes that follow more pseudo-first order kinetics, so that it further strengthens the results obtained from the adsorption isotherm which more closely follows the Freundlich isotherm that the adsorption process is physical. which means that the adsorption process does not depend on the amount of adsorbent but on the short length of the adsorption contact time [19].

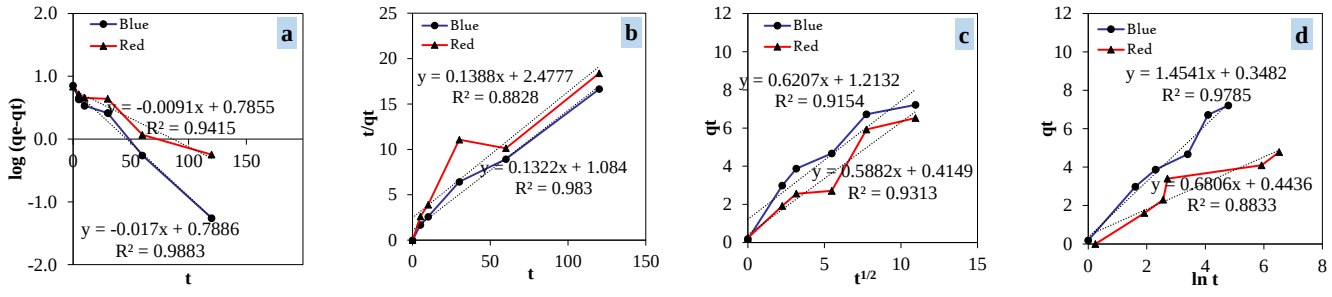

Figure 8. Kinetics adsorption of Remazol Turquoise Blue G-133 and Remazol Red RB-133 utilizing Fe_3O_4 of (a) Pseudo first-order, (b) Pseudo second-order, (c) Interparticle diffusion and (d) Elovich kinetics model

Table 3. Adsorption kinetic of Fe_3O_4 against Remazol Turquoise Blue G-133 and Remazol Red RB-133.

Kinetics models	Kinetics coefficient	Fe_3O_4
Pseudo first-order model: $\log (q_e - q_t) = \log q_e - \frac{k_1}{2.303} t$	Remazol Turquoise Blue G-133	
	q_1 ($mg.g^{-1}$)	6.15
	k_1 (min^{-1})	$-3.92x10^{-2}$

linear plot: log (q_e-q_t) vs t [20, 21].	Remazol Red RB-133	
	q_1 (mg.g^{-1})	6.10
	k_1 (min^{-1})	-2.10x10^{-2}
Pseudo second-order model: $\frac{t}{q_t} = \frac{1}{k_2 q_e^2} + \frac{1}{q_e} t$	Remazol Turquoise Blue G-133	
	q_2 (mg.g^{-1})	7.56
	k_2 (g.mg^{-1} min^{-1})	1.61x10^{-2}
	Remazol Red RB-133	
linear plot: t/q_t vs t [20, 21].	q_2 (mg.g^{-1})	7.20
	k_2 (g.mg^{-1} min^{-1})	7.78x10^{-3}
	Remazol Turquoise Blue G-133	
Intraparticle diffusion model: $q_t = k_{id} t^{1/2} + C$	C (mg.g^{-1})	1.21
	k_{id} (mg.g^{-1} min$^{-1/2}$)	6.21x10^{-1}
	Remazol Red RB-133	
linear plot: q_t vs $t^{1/2}$ [20, 21].	C (mg.g^{-1})	4.15x10^{-1}
	k_{id} (mg.g^{-1} min$^{-1/2}$)	5.88x10^{-1}
	Remazol Turquoise Blue G-133	
Elovich kinetics model: $q_t = \left(\frac{1}{\beta}\right) \ln(\alpha\beta) + \left(\frac{1}{\beta}\right) \ln(t)$	α (mg.g^{-1}. min^{-1})	1.85
	β (g.mg^{-1})	6.88x10-1
	Remazol Red RB-133	
linear plot: q_t vs ln t [20, 21].	α (mg.g^{-1}. min^{-1})	1.31
	β (g.mg^{-1})	1.47

Thermodynamics Adsorption

The determination of Remazol Turquoise Blue G-133 and Remazol Red RB-133 adsorption thermodynamics using Fe_3O_4 serves to evaluate the relationship between heat, work, and temperature, as well as its interaction with energy, radiation, and physical properties of Fe_3O_4. That is, adsorption thermodynamics is concerned with the movement of energy from one region to another and from one form to another [20, 22]. The following equations allow us to calculate the thermodynamic parameters:

$$\Delta G^o = \Delta H^o - T\Delta S^o \quad (3)$$

$$\ln \frac{q_e}{C_e} = \frac{\Delta S^O}{R} + \frac{-\Delta H^o}{R} x \frac{1}{T} \quad (4)$$

With: R: universal gas constant (8.314 J/mol.K), T: absolute temperature (K), ΔG^o: standard Gibbs free energy (J/mol), ΔH^o: standard enthalpy (J/mol), ΔS^o: entropy (J/mol.K).

According to Table 4. The thermodynamics of Fe_3O_4 adsorption against Remazol Turquoise Blue G-133 and Remazol Red RB-133 has a positive value for ΔH^o and ΔG^o, This indicates that the adsorption process with Fe_3O_4 was endothermic and not spontaneous. on the other hand, the dyes Remazol Turquoise Blue G-133 and Remazol Red RB-133, had values of ΔS^o 21.98 and 2.55 J/mol.K, respectively. A positive ΔS^o value reflects the degree of disorder in the adsorption process; Remazol Turquoise Blue G-133 has a higher ΔS^o value than Remazol Red RB-133.

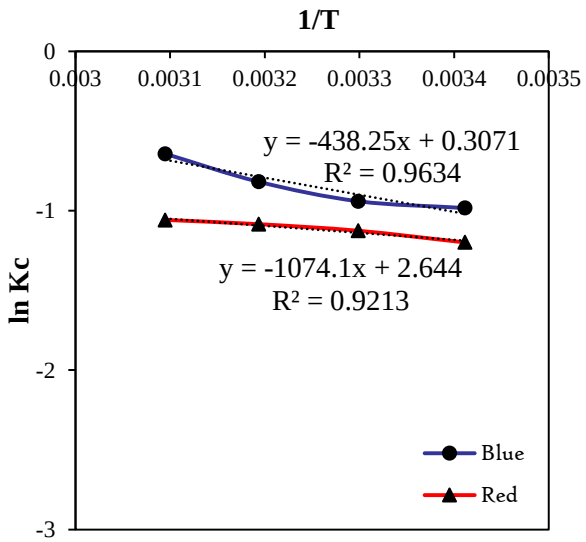

Figure 9. The Van't Hoff plots for Remazol Turquoise Blue G-133 and Remazol Red RB-133 utilizing Fe_3O_4

Table 4. Adsorption Thermodynamics coefficients of Fe_3O_4 against Remazol Turquoise Blue G-133 and Remazol Red RB-133.

Dyes (10 mg/L)	T (K)	ln (q_e/C_e)	R^2 Thermal	ΔS^o (J/mol.K)	ΔH^o (J/mol)	ΔG^o (J/mol)
Remazol Turquoise Blue G-133	293.15	-0.4269	0.9213	21.98	8929.23	2485.15
	303.15	-0.4085				2265.33
	313.15	-0.3554				2045.50
	323.15	-0.2792				1825.68
Remazol Red RB-133	293.15	-1.1982	0.9634	2.55	3643.61	2895.13
	303.15	-1.1260				2869.60
	313.15	-1.0851				2844.07
	323.15	-1.0585				2818.53

CONCLUSION

Fe_3O_4 was effectively separated using high-energy ball milling with an 81.87% yield. The reduction of silica pick on iron sand following activation with 2 M NaOH indicated the effectiveness of Fe_3O_4 separation, which was validated by SEM-EDS. The optimum pH in the adsorption test with Remazol Turquoise Blue G-133 and Remazol Red RB-133 was pH 5, with isothermal and adsorption kinetics quite following closely the Freundlich isothermal and Pseudo First order kinetics indicating that the adsorption process occurred physically, which was confirmed in adsorption thermodynamics by the ΔG^o value being positive, indicating that the adsorption process would not occur spontaneously.

ACKNOWLEDGEMENTS

I would like to offer my sincere appreciation of gratitude to my research supervisors “Dr. Fahmiati, S.Si, M.Si, M.Sc.” and “Armid, S.Si, M.Si, M.Sc, D.Sc.” for their excellent guidance and support in finishing my project, as well as providing me with all of the supporting equipment. This work was supported by the Directorate of Research, Technology, and Community Service of Indonesian Directorate General of Higher Education, Research, and Technology's. via a project of Research Thesis for Magister Student nr. 108/E5/PG.02.00. PT/2022. May, 10th 2022.

REFERENCES

[1] Gunanto, Y. E., Izaak, M. P., Jobiliong, E., Cahyadi, L. & Adi, W. (2018). High purity Fe_3O_4 from Local Iron Sand Extraction. Journal of Physics: Conference Series. 1011. 012005. Doi: 10.1088/1742 6596/1011/1/012005.

[2] Rahmawati, R., Taufiq, A., Sunaryono, S., Fuad, A., Yuliarto, B., Suyatman, S., Kurniadi, D. (2018). Synthesis of Magnetite (Fe_3O_4) Nanoparticles from Iron sands by Coprecipitation-Ultrasonic Irradiation Methods. Journal of Materials and Environmental Science. 9: 155-160. Doi: 10.26872/jmes.2018.9.1.19

[3] Ainun, N. S., Sutanto, H., Manawan, M., Setiadi, E., Wibowo, A. A., Dyan, I., Fidelia. D., Alkian, I., Hidayanto, E., Priyono, P., Marhaendrajaya, I., Triadyaksa, P. (2022). Diffraction and Magnetization Properties of Fe_3O_4 Nanoparticle from Natural Iron Sand in Various Stirring Rate for Potential Biomedical Applications. Rasayan Journal of Chemistry. Vol. 15: 316-325. Doi: 10.31788/RJC.2022.1516615

[4] Yu, Y., Guo, H., Zhong, Z., Wang, A., Xiang, M., Xu, S., Dong, C. & Chang, Z. (2022). Fe_3O_4 loaded on ball milling biochar enhanced bisphenol a removal by activating persulfate: Performance and activating mechanism. Journal of Environmental Management. Vol. 319(115661). SN-0301-4797. Doi: 10.1016/j.jenvman.2022.115661.

[5] Zhang, Z. & Wen, G. (2022). Synthesis and characterization of carbon-encapsulated magnetite, martensite and iron nanoparticles by high-energy ball milling method. Materials Characterization. Vol. 167(110502). SN -1044-5803. Doi: 10.1016/j.matchar.2020.110502

[6] Zhang, X., Tan, J., Wei, X. and Wang, L. (2013). Removal of Remazol turquoise Blue G-133 from aqueous solution using modified waste newspaper fiber. Carbohydrate Polymers. Vol. 92(2): 1497-1502. SN-0144-8617. Doi: 10.1016/j.carbpol.2012.10.066

[7] El-Boraei, N. F., Ibrahim, M.A. M. & Naghmash, M. (2022). Nanocrystalline FeNi alloy powder prepared by electrolytic synthesis; characterization and its high efficiency in removing Remazol Red dye from aqueous solution. Journal of Physics and Chemistry of Solids. Vol. 167(110714). SN - 0022-3697. Doi: 10.1016/j.jpcs.2022.110714

[8] Fahmiati, F., Nuryono, N. & Suyanta, S. (2017). Characteristics of Iron Sand Magnetic Material from Bugel Beach, Kulon Progo, Yogyakarta. IOP Conference Series: Materials Science and

Engineering. (Vol. 172, p. 12020). doi: 10.1088/1757-899X/172/1/012020

[9] Elmobarak, W. F. & Almomani, F. (2021). A new insight into the separation of oil from oil/water emulsion by Fe_3O_4–SiO_2 nanoparticles. Environmental Research, Volume 202 (111645), ISSN 0013-9351. Doi: 10.1016/j.envres.2021. 111645.

[10] Zhang, X., Chen, L., Liu, R., Li, D., Ge, X., & Ge, G. (2019). The Role of the OH Group in Citric Acid in the Coordination with Fe_3O_4 Nanoparticles. Langmuir. 35(25), 8325-8332. Doi: 10.1021/acs.langmuir.9b00208. Epub 2019 Jun 12. PMID: 31149819.

[11] Foroutan, R., Peighambardoust S. J., Peighambardoust S. H., Pateiro, M., & Lorenzo, J. M. (2021) Adsorption of Crystal Violet Dye using Activated Carbon of Lemon Wood and Activated Carbon/Fe_3O_4 Magnetic Nanocomposite from Aqueous Solutions: A Kinetic, Equilibrium and Thermodynamic Study. Molecules. 26(8):2241. Doi: 10.3390/molecules26082241. PMID: 33924445; PMCID: PMC8068907.

[12] Elmobarak, W. F. & Almomani, F. (2021). A new insight into the separation of oil from oil/water emulsion by Fe_3O_4–SiO_2 nanoparticles. Environmental Research, Volume 202 (111645), ISSN 0013-9351. Doi: 10.1016/j.envres.2021. 111645.

[13] Mohammadi, N., Khani, H., Gupta, V. K., Amereh, E., & Agarwal, S. (2011). Adsorption process of methyl orange dye onto mesoporous carbon material–kinetic and thermodynamic studies. Journal of Colloid and Interface Science. 362(2), 457-462. ISSN 0021-9797. Doi: 10.1016/j.jcis.2011.06.067.

[14] Pervez, M. N., He, W., Zarra, T., Naddeo, V., Zhao, Y. (2020). New Sustainable Approach for the Production of Fe_3O_4/Graphene Oxide-Activated Persulfate System for Dye Removal in Real Wastewater. Water. 12(3):733. Doi: 10.3390/w12030733

[15] Haseeb, A., Rova, M., & Samuelsson, J. (2023) Method development for the acquisition of adsorption isotherm of ion pair reagents Tributylamine and Triethylamine in ion pair chromatography. Journal of Chromatography A. 1687(463687). ISSN 0021-9673. Doi: 10.1016/j.chroma.2022.463687.

[16] Savka, Kh., Kilivnik, Y., Mironyuk, I., Vasylyeva, H., Sych, O., Karbovanets, M. & Yevych, M. (2023). Ba^{2+} ions adsorption by titanium silicate, Chemical Physics Impact. Vol. 6, 100151. ISSN 2667-0224. Doi: 10.1016/j.chphi.2022.100151.

[17] Dogra, I., Kumar, B. J., Etika, K. C., Chavali, M., Khalifa, A. S., Gharib, A. F. and Askary. E. A. 2022. Environmentally Friendly Low-cost Graphene Oxide-cellulose Nanocomposite Filter for Dye Removal from Water. Journal of King Saud University-Science. Vol. 34 (102122). Doi: 10.1016/j.jksus.2022.102122.

[18] Sahoo, R. T. & Prelot, B. (2020). Adsorption processes for the removal of contaminants from wastewater: the perspective role of nanomaterials and nanotechnology. In Micro and Nano Technologies, Nanomaterials for the Detection and Removal of Wastewater Pollutants. Elsevier. Pages 161-222. ISBN 9780128184899. Doi: 10.1016/B978-0-12-818489-9.00007-4.

[19] Geonzon, L. C., Kobayashi, M., Sugimoto, T. & Yasuhisa Adachi, Y. (2023). Adsorption kinetics of polyacrylamide-based polyelectrolyte onto a single silica particle studied using microfluidics and optical tweezers, Journal of Colloid and Interface Science. 630 (Part A): 846-854. ISSN 0021-9797. Doi: 10.1016/j.jcis.2022.10.067.

[20] Annon, I. A., Abbas, A. S., Al-Azzawi, W. K., Hanoon, M. M., Alamiery, A. A., Isahak, W. N. R. W. & Kadhum, A. A. H. (2022). Corrosion inhibition of mild steel in hydrochloric acid environment using thiadiazole derivative: Weight loss, thermodynamics, adsorption and computational investigations, South African Journal of Chemical Engineering. Vol 41: 244-252. ISSN 1026-9185. Doi: 10.1016/j.sajce.2022.06.011.

[21] Akpomie, K. G. and Conradie, J. 2021. Isotherm, Kinetic, Thermodynamics and Reusability Data on The Adsorption of Antidepressant onto Silver Nanoparticle-Loaded Biowaste. Journal of Data in Brief. Vol. 39 (107575). Doi: 10.1016/j.dib.2021.107575.

[22] Wang, N., Tan, Y., Xidong Du, X., & Yin, Q. (2022). Study on the difference in adsorption thermodynamics for water on swelling and non-swelling clays with implications for prevention and treatment of pneumoconiosis. Arabian Journal of Chemistry. 15(7). 103895. ISSN 1878-5352. Doi: 10.1016/j.arabjc.2022.103895.